Physical modelling of a harp from Central Africa

François Fabre, Jean-Loïc Le Carrou, Baptiste Chomette

Physical modelling of a harp from Central Africa

François Fabre,[1] Jean-Loïc Le Carrou,[1, a] and Baptiste Chomette[2]

[1]*Sorbonne Université, CNRS, Institut Jean Le Rond d'Alembert, Equipe Lutheries-Acoustique-Musique, F-75005 Paris, France*

[2]*Laboratoire de Tribologie et Dynamique des Systèmes, UMR CNRS 5513, École Centrale de Lyon, 69134 Écully, France*

Central Africa harps are string instruments, often anthropomorphic, serving an essential cultural role. Compared to pedal harps, their body is small in size with a soundboard mainly made of animal skin and a neck made of a wood beam. In this paper, a physical model is developed as a tool in assessing the specificities of these musical instruments, from a vibro-acoustic perspective. The modeling strategy is based on the modal Udwadia-Kalaba formalism which is a multibody substructuring technique. Input modal parameters of the body and the strings are experimentally identified and the main steps of the estimation procedures are detailed. The reliability of the physical model is investigated via the comparison between simulated and experimental data for several plucking configurations. Different hypotheses are assessed such as the string/neck coupling which proves to strongly influence the dynamic response of the body when there is a coincidence between string and neck modal frequencies. The inclusion of geometrical nonlinearities proves to be of major importance, even for a weak plucking, as it allows qualitative representation of phantom partials in the simulations. Overall, physical simulations of the soundboard motion are in good agreement with measurements indicating that characteristic features of the instrument are captured.

[XYZ]   **Pages: 1–12**

I. INTRODUCTION

Central Africa harps are string instruments, often anthropomorphic, with an important symbolic representation in therapeutic practices and social activities such as initiation rites[1]. These instruments reveal a great diversity in terms of repertoires, designations and morphological and acoustic characteristics, as much nowadays as under historical form in museums. Despite this diversity, different studies have shown that groupings are possible based on organological, ethnomusicological and linguistic descriptors[2]. A preliminary vibro-acoustic study based on 3 Gabonese harps has been published[3], the ratio of eigenfrequencies showed that 2 harps have a plate-like vibratory behavior while that of the third harp was membrane-like. In the continuity of this work, the present paper deals with the development of a physical model as a tool in assessing the specificities of a Central Africa harp, from a vibro-acoustic perspective.

From a design perspective, Central Africa harps consist in four key components: the 5 to 11 strings, the neck, the soundboard and the soundbox. The soundbox is made of a tree trunk hollowed out using manual tools such as an ax, a machete or a chisel. The strings are bound, at one end, to wooden tuning pegs going across the neck, and at the other, coupled to the soundboard, through a tailpiece placed under it. Among constitutive materials, regarding the soundboard, the most common

is animal skin, such as antelope or gazelle, but specimens were also found with a metal sheet or a plastic tarpaulin. Strings were formerly made of animal gut or plant based materials but harp-makers have now moved to fishing lines made of nylon. In this paper, a harp from the Fang ethnic group is studied as it gives a good representation of Central Africa harps in term of dimensions and sophistication of assembly. It is presented in playing conditions in Fig 1(a). Its soundboard is covered with a coat of white paint and measures approximately 50 cm of high and 10 cm to 3 cm of width with a trapezoidal shape. Its neck of length 45 cm is fitted in the top of the soundbox and tied to it with a metallic wire.

The literature on the acoustics of the harp includes a wide range of studies of which an overview is given by Waltham[4]. A study of the strings/soundboard coupling[5] has shown the crucial relation between the position of antinodes of soundboard's mode shapes, the strings' attachment points and the evolution of strings' and soundboard's modal frequencies regarding the evenness of sound production over all strings. This coupling was also investigated in the context of sympathetic vibrations between strings by developing an analytical model[6]. The latter highlighted the presence of string-string modes in the complete structure. Another recent study[7] focused on the existence of a characteristic "harp sound" and sought its origins in the unusual physical configuration with respect to other plucked-string instruments. A nonlinear model of string/soundboard coupling allowed to point out the strong influence of the string/soundboard angle on the sound through the excitation of longitudi-

---
[a]jean-loic.le_carrou@sorbonne-universite.fr

nal string vibrations. This phenomena was studied earlier by Boutillon[8] as a general feature of stiff strings. The coupling between the soundboard and the air cavity inside the soundbox in the low frequency range has been studied in the case of a Camac Atlantide Prestige concert harp[9]. Global modes associated with breathing modes of the cavity were shown to be the most important acoustically. Above the modal frequencies of these modes, the modal behavior of the uncoupled soundboard remains but is shifted up in frequency[5]. Another work found the sound radiation from concert harps to be omnidirectional below 200 Hz and becoming more complex with increasing frequency[10,11]. Finally, string choice was also addressed[12,13] in term of constitutive material properties and gauge of plain strings.

With a view to developing a physical model allowing to study the influence of coupling conditions at the string ends in multiple polarizations, different methods have shown promising results. Woodhouse[14] compared different formulations (both in time and frequency domain) when applied to the case of plucked guitar strings, he emphasized the simplicity and efficiency of the frequency domain formulation by means of a coupling admittance. Although this avoids the need for a proper modal parameters estimation of substructures, a frequency domain formulation is not suited for nonlinear behaviors. In the time domain, Antunes and Debut recently adapted the Udwadia-Kalaba (U-K) formulation[15,16], originally suited for rigid multibody systems, to flexible coupled systems by describing them through their uncoupled modal basis[17]. Recent studies showed the ability of this formulation to include string nonlinearities[18] (guitar), collisions[19] and sympathetic vibrations[20] in the case of the clavichord. Following these results, it seemed appropriate to include multiple string polarizations as well as coupling with the instrument's body at both ends. It should be noted that other approaches based on finite differences/elements exist in the literature[21] but are not in the frame of the present study.

The paper is structured as follows: first, section II presents the harp model in terms of the U-K modal formalism, followed by the approach considered to take into account geometrical nonlinearities. Section III then deals with the modal parameters estimation of the harp body and the strings which are input parameters of the model. This includes the description of the identification procedures and the experimentally identified modal parameters. Finally, in section IV, numerical simulations are confronted to measurements with a view to validating the harp model. The latter is then used to determine characteristic features responsible for the vibro-acoustic signature of the instrument.

II. HARP MODEL

In this section, the harp model, which will lead to the simulations of section IV, is presented. The substructuring concept on which it relies is of particular interest for its ability to study each instrument-making
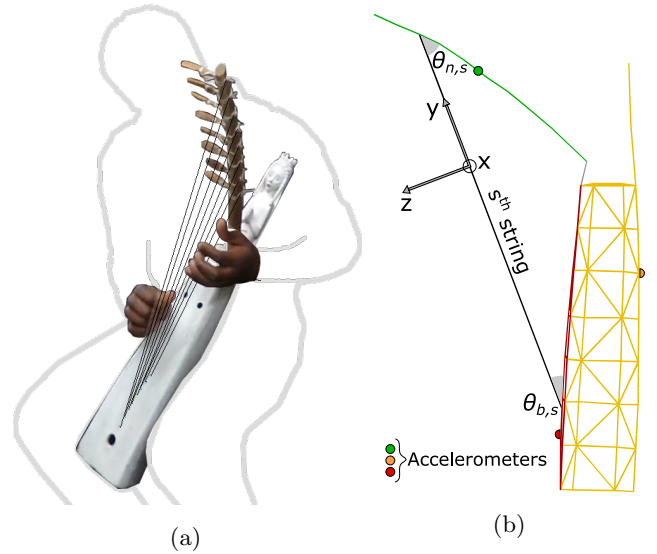

Figure 1. (Color online) (a) Central Africa harp (Fang ethnic group) in playing condition; (b) 3D mesh of the physical model. The local coordinate system illustrates strings' polarizations.

component independently. In the frame of this study, the harp is split into 2 groups: the N_s strings and the body (including the neck, the soundboard and the soundbox) as represented in Fig. 1(b). The strings are further decomposed into two categories, each correspond to a transverse polarization of vibration. The following notations are used: s denotes the sth string, W denotes any string transverse polarization; B denotes the body with b for the tailpiece and n for the neck; $\theta_{n,s}$ and $\theta_{b,s}$ denote the angles that makes the sth string with, respectively, the neck and the tailpiece. The harp model presented below will allow to test different hypothesis regarding the influence of strings' features such as string/neck coupling, the number of vibrating polarizations and the inclusions of geometrical nonlinearities.

A. General U-K formalism

Let $\mathbf{x}(t)$ represent the response of a discrete mechanical system of mass matrix $\mathbf{M}$, which consists of L constrained sub-systems via constraining forces $\mathbf{F}_c$, subjected to constraint-independent forces $\mathbf{F}$. Udwadia-Kalaba formulation (U-K) derives from

$$\mathbf{M}\ddot{\mathbf{x}} = \mathbf{F}(\mathbf{x}, \dot{\mathbf{x}}, t) + \mathbf{F}_c(\mathbf{x}, \dot{\mathbf{x}}, t). \qquad (1)$$

Constraining forces can be expressed through Lagrange multipliers[22] λ as

$$\mathbf{F}_c = -\mathbf{A}^T \lambda \text{ with } \mathbf{A}\ddot{\mathbf{x}} = \mathbf{b} \qquad (2)$$

where $\mathbf{A}$ is the constraint Jacobian matrix, associated with $\mathbf{b}$ a vector function of the motion, corresponding to a system of P constraints in terms of accelerations.

The main result from Udwadia and Kalaba[15,16] resides in the explicit expression of the constraining forces, leading to the dynamic response of the constrained system from the unconstrained one $\mathbf{x}_u$ to which a correction is added

$$\ddot{\mathbf{x}} = \underbrace{\ddot{\mathbf{x}}_u}_{\mathbf{M}^{-1}\mathbf{F}} + \underbrace{\mathbf{M}^{-1/2}\mathbf{B}^\dagger(\mathbf{b} - \mathbf{A}\ddot{\mathbf{x}}_u)}_{\mathbf{M}^{-1}\mathbf{F}_c} \qquad (3)$$

with $\mathbf{B}^\dagger$ denoting the Moore-Penrose pseudo-inverse of $\mathbf{B} = \mathbf{A}\mathbf{M}^{-1/2}$.

From this point, Antunes & Debut[17] adapted the U-K formulation to continuous flexible systems by means of modal coordinates. In a similar manner to Eq. 3, they obtained, in the modal space, the following expression for the modal response $\boldsymbol{q}$ of the constrained system

$$\ddot{\boldsymbol{q}} = \ddot{\boldsymbol{q}}_u + \boldsymbol{M}^{-1/2}\boldsymbol{B}^\dagger(\mathbf{b} - \boldsymbol{A}\ddot{\boldsymbol{q}}_u). \qquad (4)$$

$\boldsymbol{q}_u$ being the modal response of the unconstrained system, $\boldsymbol{M}$ the modal mass matrix, $\boldsymbol{A} = \mathbf{A}\boldsymbol{\Phi}$ the modal constraint Jacobian matrix, $\boldsymbol{\Phi}$ a matrix containing the mode shapes of all subsystems on its diagonal and $\boldsymbol{B} = \boldsymbol{A}\boldsymbol{M}^{-1/2}$.

Thus, if we further details the assembly of vectors and matrices in Eq. 4, we obtain

$$\boldsymbol{q} = \begin{Bmatrix} \boldsymbol{q}^1 \\ \vdots \\ \boldsymbol{q}^L \end{Bmatrix}, \boldsymbol{q}_u = \begin{Bmatrix} \boldsymbol{q}_u^1 \\ \vdots \\ \boldsymbol{q}_u^L \end{Bmatrix}, \boldsymbol{M} = \begin{bmatrix} \boldsymbol{M}^1 & \cdots & \mathbf{0} \\ \vdots & \ddots & \vdots \\ \mathbf{0} & \cdots & \boldsymbol{M}^L \end{bmatrix}, \boldsymbol{A} = \begin{bmatrix} \boldsymbol{A}^1 \\ \vdots \\ \boldsymbol{A}^P \end{bmatrix} \qquad (5)$$

where the modal response of a specific unconstrained system of modal mass, damping and stiffness matrices $\boldsymbol{M}^s$, $\boldsymbol{C}^s$ and $\boldsymbol{K}^s$, subjected to modal forces $\boldsymbol{F}_{\text{ext}}^s$, is given by

$$\ddot{\boldsymbol{q}}_u^l = \left(\boldsymbol{M}^l\right)^{-1}\left(-\boldsymbol{C}^l\dot{\boldsymbol{q}}^l - \boldsymbol{K}^l\boldsymbol{q}^l + \boldsymbol{F}_{\text{ext}}^l\right). \qquad (6)$$

B. Application to the harp

Substructuring the harp as described above, the fully coupled model consists in 3 systems. The first two subsystems correspond to the N_s strings in both polarizations (denoted, respectively, X and Z). The last one refers to the harp body (denoted B). Depending on the different strings' coupling conditions included, the mode shapes of the soundboard and the neck can have components in multiple spatial directions. To allow for the coupling of the strings to the body at both ends, the modal basis of a free-free string is considered. Mode shapes ϕ_k^W are thus written

$$\phi_k^W(y) = \cos\left(\frac{k\pi y}{L}\right), \quad k = 0, ..., N_W - 1. \qquad (7)$$

From Eq. 6, the modal response of the unconstrained subsystems of the full harp model is

$$\begin{Bmatrix} \ddot{\boldsymbol{q}}_u^X \\ \ddot{\boldsymbol{q}}_u^Z \\ \ddot{\boldsymbol{q}}_u^B \end{Bmatrix} = \begin{bmatrix} \boldsymbol{M}^X & 0 & 0 \\ 0 & \boldsymbol{M}^Z & 0 \\ 0 & 0 & \boldsymbol{M}^B \end{bmatrix}^{-1} \left(-\begin{bmatrix} \boldsymbol{C}^X & 0 & 0 \\ 0 & \boldsymbol{C}^Z & 0 \\ 0 & 0 & \boldsymbol{C}^B \end{bmatrix} \begin{Bmatrix} \dot{\boldsymbol{q}}_u^X \\ \dot{\boldsymbol{q}}_u^Z \\ \dot{\boldsymbol{q}}_u^B \end{Bmatrix} \right.$$
$$\left. -\begin{bmatrix} \boldsymbol{K}^X & 0 & 0 \\ 0 & \boldsymbol{K}^Z & 0 \\ 0 & 0 & \boldsymbol{K}^B \end{bmatrix} \begin{Bmatrix} \boldsymbol{q}_u^X \\ \boldsymbol{q}_u^Z \\ \boldsymbol{q}_u^B \end{Bmatrix} + \begin{Bmatrix} \boldsymbol{F}_{\text{ext}}^X \\ \boldsymbol{F}_{\text{ext}}^Z \\ \mathbf{0} \end{Bmatrix} \right) \qquad (8)$$

Then the different boundary conditions of the strings are taken into account through the modal constraint Jacobian matrix $\boldsymbol{A}$ as described in Eq. 10. First, let us define mode shape amplitudes in the polarization W:

- $\phi_b^{W_s}$ of the sth string at the tailpiece
- $\phi_n^{W_s}$ of the sth string at the neck
- $\phi_s^{W_b}$ of the tailpiece at the sth string
- $\phi_s^{W_n}$ of the neck at the sth string.

Figure 2 shows a comparison of direct and cross accelerance measured at the attachment point of the 8th string on the soundboard. One should notice that the difference in magnitude between A_Z/F_Z and A_X/F_X is approximately 10 to 50 dB for frequencies below 1600 Hz (indicated by the vertical gray dashed line), except for a resonance at 108 Hz and around 600 Hz and 1100 Hz. The same remark can be made about A_X/F_Z despite a closer trend. Considering the difficulties occurring in the identification of tangential mode shape components of the soundboard, in the following it is assumed that strings/soundboard coupling only occurs in the perpendicular direction to the soundboard.
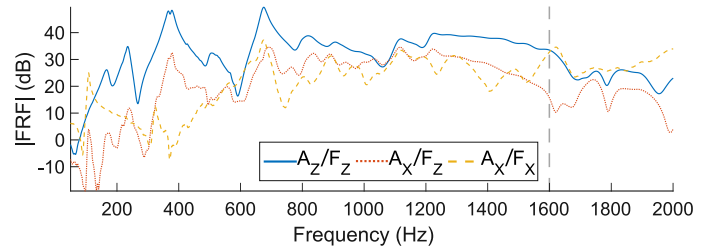

Figure 2. (Color online) Comparison of direct and cross accelerances on the soundboard at the attachment point of the 8th string. The direct acceleration in the perpendicular direction Z is denoted A_Z/F_Z, the one in the tangential direction X is denoted A_X/F_X and the cross acceleration is denoted A_X/F_Z.

Coupling conditions between the strings and the body are thus written at the acceleration level

$$\begin{bmatrix} \phi_b^{X_s}\ddot{\boldsymbol{q}}^{X_s} \\ \phi_n^{X_s}\ddot{\boldsymbol{q}}^{X_s} \\ \phi_b^{Z_s}\ddot{\boldsymbol{q}}^{Z_s} \\ \phi_n^{Z_s}\ddot{\boldsymbol{q}}^{Z_s} \end{bmatrix} = \begin{bmatrix} \mathbf{0} \\ \phi_s^{X_n}\ddot{\boldsymbol{q}}^B \\ \cos(\theta_{b,s})\phi_s^{Z_b}\ddot{\boldsymbol{q}}^B \\ \cos(\theta_{n,s})\phi_s^{Z_n}\ddot{\boldsymbol{q}}^B \end{bmatrix}, \quad s = 1, ..., N_s. \quad (9)$$

Using a matrix formulation, this set of equation can be restated to show the corresponding modal constraint Jacobian matrix $\boldsymbol{A}$

$$\boldsymbol{A}\ddot{\boldsymbol{q}} = \begin{bmatrix} \boldsymbol{\Phi}_b^X & \boldsymbol{0} & \boldsymbol{0} \\ \boldsymbol{\Phi}_n^X & \boldsymbol{0} & -\boldsymbol{\Phi}^{X_n} \\ \boldsymbol{0} & \boldsymbol{\Phi}_b^Z & -\boldsymbol{\Phi}^{Z_b}\cos(\boldsymbol{\Theta}_b) \\ \boldsymbol{0} & \boldsymbol{\Phi}_n^Z & -\boldsymbol{\Phi}^{Z_n}\cos(\boldsymbol{\Theta}_n) \end{bmatrix} \begin{Bmatrix} \ddot{\boldsymbol{q}}^X \\ \ddot{\boldsymbol{q}}^Z \\ \ddot{\boldsymbol{q}}^B \end{Bmatrix} = \begin{Bmatrix} \boldsymbol{0} \\ \boldsymbol{0} \\ \boldsymbol{0} \\ \boldsymbol{0} \end{Bmatrix} \quad (10)$$

with the following mode shapes matrices

$$\boldsymbol{\Phi}_*^W = \begin{bmatrix} \phi_*^{W_1} & \cdots & \boldsymbol{0} \\ \vdots & \ddots & \boldsymbol{0} \\ \boldsymbol{0} & \boldsymbol{0} & \phi_*^{W_{N_s}} \end{bmatrix}, \boldsymbol{\Phi}^{Z_*} = \begin{bmatrix} \phi_1^{Z_*} \\ \vdots \\ \phi_{N_s}^{Z_*} \end{bmatrix} \quad (11)$$

and

$$\boldsymbol{\Theta}_* = \begin{bmatrix} \theta_{*,1} & \cdots & \boldsymbol{0} \\ \vdots & \ddots & \boldsymbol{0} \\ \boldsymbol{0} & \boldsymbol{0} & \theta_{*,N_s} \end{bmatrix}, * \text{ can be either n or b.} \quad (12)$$

As a remark, setting $\boldsymbol{\Phi}^{Z_n}$ and $\boldsymbol{\Phi}^{X_n}$ to the null matrix leads to rigid boundary conditions at the neck for the strings which will be done in section IV.

The combination of Eqs. 8 and 10 in Eq. 4 forms the fully coupled harp model.

C. String geometrical nonlinearities

Nonlinear polarization coupling in string vibrations have been observed in many musical instruments either due to high initial string displacement or to coupling with the instrument body. This is particularly likely to happen in Central Africa harps since in several ceremonies, the harp is at the center of a musical piece, accompanied by percussion instruments, and has to be distinguishable which requires the harpist to play louder by strongly plucking the strings. Soundboard acceleration responses (to a plucking performed by a Gabonese harpist) indeed revealed a non-negligible pitch glide, right after the plucking. In order to include these nonlinear phenomenons in our physical model, Kirchhoff-Carrier model[23,24] is implemented.

1. Transverse polarizations coupling

This model relies on the fact that when the speed of longitudinal waves is much larger than that of the transverse ones ($ES \gg T_0$) the dynamic tension induced by the transverse displacement is uniform along the string. The free transverse vibrations of such a string obey the following equation[23,24]

$$\rho S \frac{\partial^2 W}{\partial t^2} = [T_0 + T_{\mathrm{dyn}}] \frac{\partial^2 W}{\partial y^2} \quad (13)$$

with the dynamic tension

$$T_{\mathrm{dyn}} = \frac{ES}{2L} \int_L \left(\frac{\partial X}{\partial y}^2 + \frac{\partial Z}{\partial y}^2 \right) dy . \quad (14)$$

The nonlinear forcing term induced by the dynamic tension in Eq. 13 is projected on the modal basis by

$$f_k^W = \int_L \left[T_{\mathrm{dyn}} \frac{\partial^2 W}{\partial y^2} \right] \phi_k^W \, dy. \quad (15)$$

Combining Eqs. 15, 14 and 7, for mode k, leads to

$$f_k^W = -\frac{ES\pi^4}{8L^3} k^2 q_k^W \left[\sum_{m=0}^{N_X-1} \left(m \, q_m^X \right)^2 + \sum_{m=0}^{N_Z-1} \left(m \, q_m^Z \right)^2 \right] \quad (16)$$

with N_X and N_Z the number of modes describing string polarizations X and Z.

The modal nonlinear efforts can be assembled to the global vector $\boldsymbol{F}_{\mathrm{nl}}^W = \left\{ f_1^W \ \cdots \ f_{N_W}^W \right\}^T$ and included in the model for a given string as

$$\boldsymbol{F}_{\mathrm{ext}}^{W_s} = \boldsymbol{F}_{\mathrm{exc}}^{W_s} + \boldsymbol{F}_{\mathrm{nl}}^{W_s}. \quad (17)$$

The term $\boldsymbol{F}_{\mathrm{exc}}^{W_s}$ corresponds to the modal excitation force vector applied on the sth string in the generic polarization W.

2. Approximation of longitudinal polarization's influence

Longitudinal string vibrations have been shown to strongly influence the sound signature of several instruments[7,25,26]. As a simple approach, a one way coupling of the (pinned-pinned) string polarization Y with the body is included through the application of the longitudinal force, at both string ends, as an external force on the body after proper projection. Given the free-free boundary conditions of string transverse polarizations, the slope at each end is null which implies that the longitudinal force is simply the dynamic tension T_{dyn}.

Now that the model is derived, one still need to determine realistic input parameters of the unconstrained strings and the body of the harp. This issue is dealt with in the next section.

III. MODAL PARAMETERS ESTIMATION

As discussed in section II, to simulate the vibratory behavior of the full harp, modal parameters of each subsystem have to be known before the application of couplings. Regarding the uncoupled strings (free-free boundary conditions), analytical solutions are well known in the literature and will be recalled in subsection III B. However, the complexity of constitutive materials of the body makes an analytical approach not an option. Thus, modal parameters are instead obtained via experimental modal analysis whose steps, in terms of experimental configuration and signal processing, are described in the next subsection.
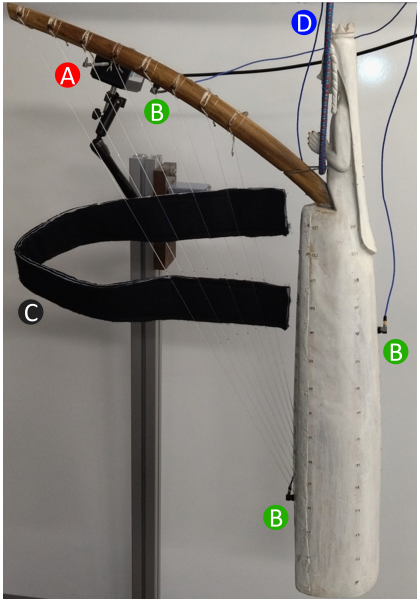
Figure 3. (Color online) Experimental setup. Ⓐ: Automatic hammer; Ⓑ: Accelerometers; Ⓒ: Strip of felt; Ⓓ: Bungee cord.

A. Modal analysis of the body

1. Experimental setup

The experimental setup shown in Fig. 3 consists in the harp hanging by means of bungee cords to approximate free boundary conditions. Strings are mounted on the harp in order to keep the static coupling with the body but a strip of felt is intertwined with them to dampen their transverse vibrations. The vibratory behavior of the body is obtained through frequency response functions (FRF) measured using a roving automatic impact hammer (force sensor PCB 086E80) and three reference accelerometers (PCB M352C65) placed at the coupling point of the fourth string with the neck, at the coupling of the eighth string with the tailpiece and in the middle of the back of the soundbox as shown in Fig. 3. The harp is impacted over the full body creating a mesh of 68 points (soundboard: 21, neck: 6, soundbox: 41) in order to visualize the mode shapes at the end of the modal parameters estimation procedure.

2. Modal parameters estimation

The identification procedure aims to determine the modal parameters required for the Udwadia-Kalaba modal formulation: natural frequency, modal damping factor, modes and modal mass. A detailed description of the different steps seems appropriate to the authors with specific attention paid to the estimation of mode shapes and modal masses. This procedure is divided into two points: firstly, poles are identified using a discrete-time-z-model and secondly mode shapes and modal masses are calculated using a continuous pole-residue model.

a. Poles identification. Poles are identified via the Linear Square Complex Frequency estimator[27] (LSCF) using a discrete-time z-model of order m.

$$\mathbf{H}(\mathbf{z}) = \frac{\sum_{k=0}^{m} \mathbf{A} z^k}{\sum_{k=0}^{m} \mathbf{B} z^k} \text{ with } z^k = e^{j\,k\,\omega\,dt} \qquad (18)$$

where $\mathbf{H}(\mathbf{z})$ is a vector of measured frequency response functions in the frequency range $[f_{start}, f_{end}]$, $dt = 1/(2\,(f_{end} - f_{start}))$ and ω the natural frequency vector. $\mathbf{A}$ and $\mathbf{B}$ are coefficient vectors to be estimated. Poles are then obtained from the companion matrix built from the denominator coefficient vector $\mathbf{B}$.

b. Mode shapes and modal masses identification. Residues are identified using the Least Square Frequency Domain estimator[27] (LSFD). Assuming a viscous structural damping, the frequency response function between an acceleration sensor located at point i and an actuator located at point j can be written for n modes using the so-called pole-residue model including lower (LR) and upper (UR) residual terms

$$H_{ij}(s) = s^2 \left[\sum_{k=1}^{n} \frac{r_{ijk}}{s - \lambda_k} + \frac{r_{ijk}^*}{s - \lambda_k^*} + \frac{LR_{ij}}{s} + UR_{ij} \right]$$
$$(19)$$

where $s = j\omega$ is the Laplace variable. * denotes the complex conjugate. r_{ijk} and $\lambda_k = \omega_k \left(-\xi_k \pm j\sqrt{1 - \xi_k^2} \right)$ are the residue and the pole of the kth mode respectively. In practice, the complex residues r_{ijk} and the upper and lower residual terms LR_{ij} and UR_{ij} are obtained by solving the linear least squares problem for each value of s and using the identified physical poles.

Complex mode shape $\boldsymbol{\psi}_k$ can be estimated, using residues of Eq. 19 by means of the singular value decomposition technique $\mathbf{R}_k = \mathbf{U}_k \boldsymbol{\Sigma}_k \mathbf{V}_k^{T}$[27]. The complex residues matrix $\mathbf{R}_k$, for each mode k, is defined by

$$\mathbf{R}_k = \begin{bmatrix} r_{11k} & \cdots & r_{1n_ak} \\ \vdots & \ddots & \vdots \\ r_{n_s1k} & \cdots & r_{n_sn_ak} \end{bmatrix} \qquad (20)$$

where n_s and n_a are, respectively, the number of sensors and actuators. Assuming the rank of $\mathbf{R}_k$ is 1 (i.e. only one singular value of $\boldsymbol{\Sigma}_k$ different from zero), the first column of $\mathbf{U}_k$ represents the complex mode shape vector $\boldsymbol{\psi}_k$ and the first row of $\mathbf{V}_k^{T}$ represents the modal participation factor. Scaled complex modes $\tilde{\boldsymbol{\psi}}_k = \boldsymbol{\psi}_k S_k^{-1/2}$ are obtained by solving a linear least squares problem on the diagonal scaling matrix S_k to verify the normalization property $\tilde{\boldsymbol{\psi}}_{ik}\tilde{\boldsymbol{\psi}}_{jk} = r_{ijk}$ for each mode k. This allows to approximate mass normalized real modes $\boldsymbol{\phi}_k$[28] using

$$\boldsymbol{\phi}_k = \Re\left(\tilde{\boldsymbol{\psi}}_k \sqrt{2j\omega_k\sqrt{1 - \xi_k^2}} \right). \qquad (21)$$

In order to check mass normalization, Eq. 19 can be written using real modes at point i and j defined by ϕ_{ik} and ϕ_{jk} as follows

$$H_{ij}(s) = s^2 \left[\sum_{k=1}^{n} \frac{\phi_{ik}\phi_{jk}}{m_k\left(s^2 + 2s\xi_k\omega_k + \omega_k^2\right)} + \frac{LR_{ij}}{s} + UR_{ij} \right]$$

(22)

where m_k is the modal mass of mode k depending on the normalization of the modes. Moreover, assuming proportional damping (i.e. pure imaginary residue) and using the definition of the poles, Eq. (19) can be rewritten

$$H_{ij}(s) = s^2 \left[\sum_{k=1}^{n} \frac{-2\Im(\lambda_k)\Im(r_{ijk})}{s^2 + 2s\xi_k\omega_k + \omega_k^2} + \frac{LR_{ij}}{s} + UR_{ij} \right].$$

(23)

Eqs. (23) and (22) thus allow to calculate the kth modal mass m_k using

$$m_k = -\frac{\phi_{ik}\phi_{jk}}{2\,\Im(\lambda_k)\Im(r_{ijk})} = -\frac{\phi_{ik}\phi_{jk}}{2\,\omega_k\sqrt{1-\xi_k^2}\,\Im(r_{ijk})}.$$

(24)

In practice, Eq. (24) is written for all the measured frequency response functions ($i \in [1, n_s]$ and $j \in [1, n_a]$) and modal mass are obtained by solving a linear least squares problem for each mode k. This procedure gives a criterion to assess the accuracy of estimated mode shapes. If estimated modal masses are not unitary, real mode shapes are found to be biased.

3. Results

Figure 4 shows reference measurements (collocated acceleration at the 3 accelerometers locations) as well as the reconstructed ones from the estimated modal parameters (see Fig. 5) using Eq. 22. The frequency axis is limited to [50,1200] Hz since no satisfactory identification was obtained above. It appears that some modes are missing on certain reconstructions (indicated by black dots) suggesting a bias in the poles identified by LSCF. However, this comparison between measured and reconstructed collocated acceleration gives us confidence in the estimated modal parameters to represent satisfactorily the dynamic behavior of the Fang harp, considering the complexity of this musical instrument.

These modal parameters are given in Fig. 5. Most mode shapes of the full body are combinations of modes of the separated elements. For example, the soundboard exhibits a membrane-like behavior[3] with bending and rolling modes, while the neck behaves like a fixed-free beam. Modes 2 and 3 exhibit very similar mode shapes which indicates the presence of a vibroacoustic coupling between the first soundboard modes (with a closed cavity) and the first acoustic mode of the cavity inside the soundbox[9]. Modes with a contribution in terms of the first rolling mode for the soundboard are expected to be very weakly coupled to the strings due to the presence of a nodal line covering the attachment points. On the other hand, for the second and third bending mode contributions (modes 2, 3, 4, 5, 6 and 7), the attachment
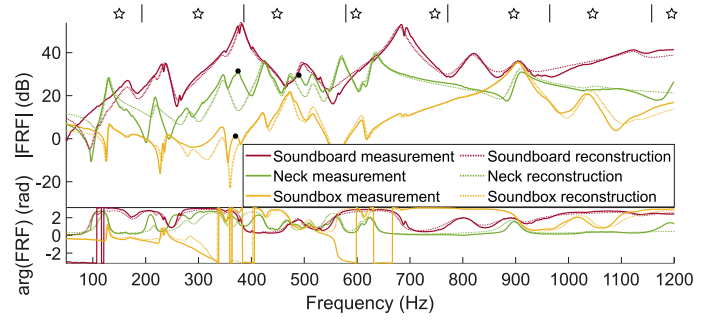
Figure 4. (Color online) Measured and reconstructed collocated accelerances on the soundboard, the neck and the soundbox of the Fang harp. Black dots indicate resonances missing in the reconstructions; Stars and vertical bars indicate modal frequencies of the 8th and 5th strings, each tuned at 149.4 Hz and 192.6 Hz.

points move in phase which may favor sympathetic coupling between the strings. The same remark can be made about mode 14 for which the string/soundboard coupling points are split in two groups moving in opposite phase. Looking at Fig. 4, it appears indeed that second and third bending modes contribute the most to the response of the soundboard at the attachment point of the 8th string.

Figure 6 shows the amplitude of body mode shapes at the attachment points of the 8th and 5th strings used in later simulations.

B. Modal analysis of the strings

Stiff string's modal parameters are known[29] from second order analytical models. The modal mass, natural frequency and modal damping are expressed for a given vibration mode of order k and free-free boundary conditions, $m_k = \rho\pi a^2 L/(2 - \delta_k^0)$, $\omega_k^W = (k\pi/L)c_t\sqrt{1 + EIk^2}$ and $c_k = 2m_k\xi_k\omega_k$. L is the length of the string, a its radius, ρ its density, c_t its transverse wave velocity, $E^* = E(1 + j\eta_E)$ the complex Young modulus, I the moment of inertia and ξ_k the modal damping factor. δ_k^0 is the Dirac function equal to 1 for $k = 0$ and 0 otherwise.

A model proposed by Woodhouse[30] is considered in our model to take into account damping mechanisms. Energy losses are split into three main categories: loss by coupling to the body, internal loss from the viscoelactic behavior and loss due to air friction. Associated loss factors for a string of fundamental frequency f_1 are expressed[30]

$$\eta_k^{\text{body}} = \frac{4\rho L f_1 a^2}{k Z_{\text{body}}}, \quad \eta_k^{\text{bend}} = \frac{E\eta_E I p_k^2}{T},$$

$$\eta_k^{\text{air}} = \frac{\rho_a}{\rho}\frac{2\sqrt{2}M + 1}{M^2} \text{ with } M = \frac{a}{2}\sqrt{\frac{2\pi f_k}{\eta_a}}.$$

(25)

p_k is the wavenumber associated with mode k. ρ_a and η_a are, respectively, the density and the cinematic viscosity

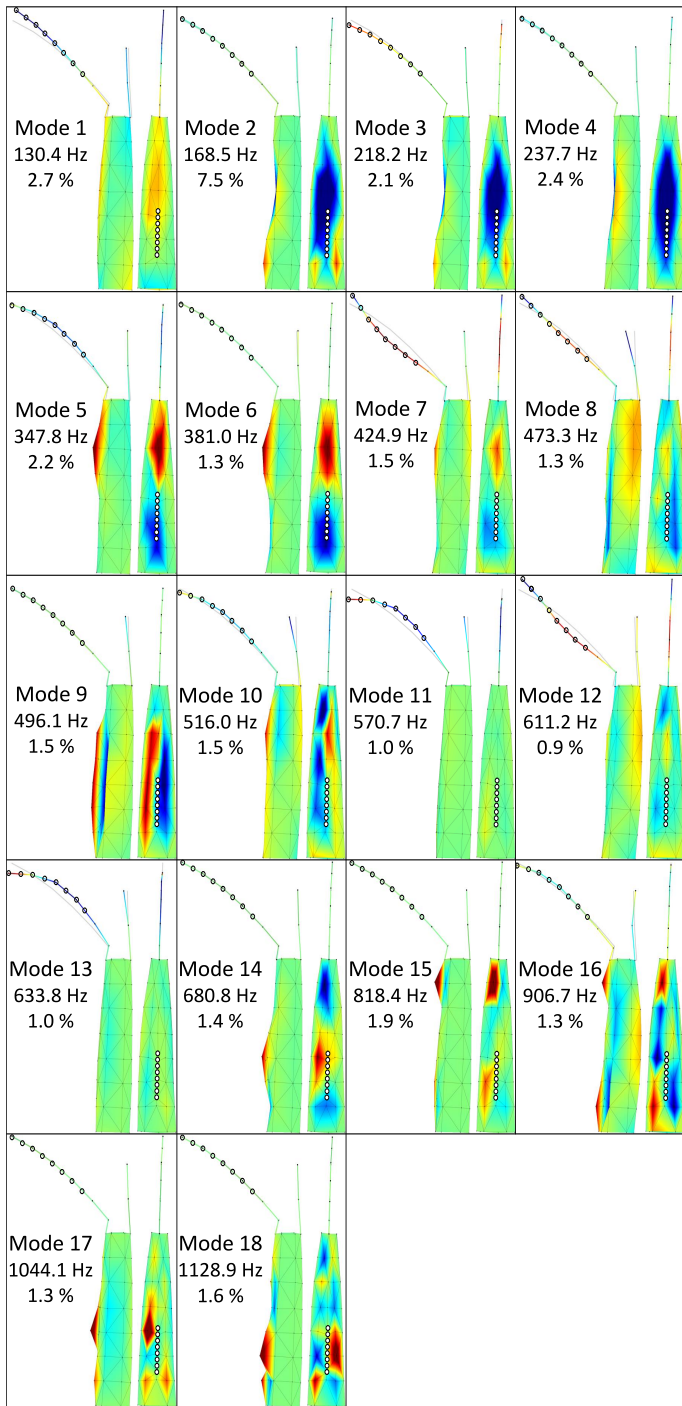Figure 5. (Color online) Experimentally identified mode shapes of a Fang harp. Black circles indicate strings' attachment points.

of air. Z_{body} is the average resistance felt by the string at its boundaries.

The modal quality factor and modal damping factor for mode k are thus

$$Q_k = \frac{1}{\eta_k^{\text{body}} + \eta_k^{\text{bend}} + \eta_k^{\text{air}}} \text{ and } \xi_k = \frac{1}{2Q_k}. \qquad (26)$$
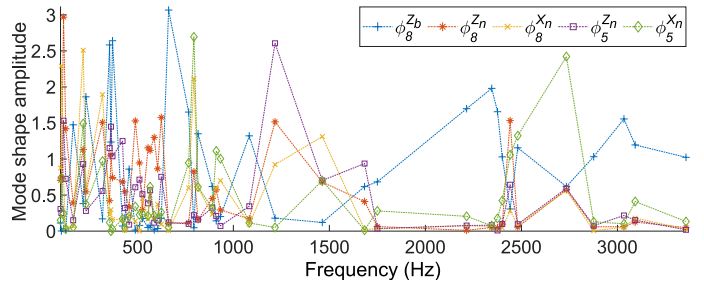

Figure 6. (Color online) Amplitude of neck and soundboard mode shapes at the attachment point of the 8th and 5th strings in X and Z string polarizations.

Quantities involved in this damping model can be easily obtained from geometrical measurements or imposed numerically. A starting value of η_E to be adjusted in the simulations is obtained, together with Z_{body}, by curve fitting this model to experimental data. The data are obtained from string displacement measurements on a string bench using optical forks[31] mounted close to one end and a wire-break plucking at the other end. The high resolution algorithm ESPRIT[32,33] is then used to estimate modal quality factors and eigenfrequencies.

IV. PHYSICAL SIMULATIONS AND EXPLOITATION

1. Simulation parameters

In this section, the validity of the physical model is investigated via the comparison between simulated and experimental data. A velocity verlet finite difference scheme[17] is used to solve for the dynamic response of unconstrained components of the model (Eq. 8). A sampling frequency of 400 kHz alongside 150 modes for each string polarization proved to be sufficient to achieve convergence. The experimental data consists in the acceleration signal measured on the Fang harp at the attachment point of the 8th string on the soundboard. When a string was plucked, the other strings were damped using a strip of felt as shown in Fig. 3.

In all later simulations, the plucking is represented in the model by a point force whose temporal envelop is a ramp of 2 seconds with an instantaneous return to 0 N. No improvement could be noticed when considering a more realistic time distribution. The adjustment variable is the maximal amplitude.

The string tension is adjusted in the model to match the tuning frequency of 153 Hz for the 8th string and 192.6 Hz for the 5th string. A value of 7.4 Gpa is used for Young modulus. Geometrical parameters of the strings used in the physical simulations are listed in table I.

R (mm)	L (cm)	$\theta_{n,8}$ (°)	$\theta_{b,8}$ (°)	$\theta_{n,5}$ (°)	$\theta_{b,5}$ (°)
0.41	69.8 — 57.3	25.6	41.0	41.4	25.5

Table I. Geometrical parameters of the 8th and 5th.

2. Cases investigated

In section IV 3, four model/measurement comparisons are presented for the following experimental configurations:

(i) the 8th string is excited at its center, in its transverse direction Z, by means of a breaking wire (0.9 mm in diameter),

(ii) the 5th string is excited at the third (from the soundboard), with a 45° angle with respect to the Z string polarization, by means of a breaking wire (0.9 mm in diameter),

(iii) same as case (i) but the breaking wire excitation is replaced by a forefinger plucking to include the low-pass filtering induced by the spatial distribution of the plucking,

(iv) the 8th string is now strongly plucked at the third (from the soundboard), with a 45° angle with respect to the Z string polarization, by a forefinger plucking to get closer to playing conditions.

3. Exploitation

In order to assess the influence of the different hypotheses available in our model, several simulated signals for case (i), with an increasing degree of complexity, are compared to a measurement in Fig. 7.

Independently of the hypotheses included in the simulation a good agreement is found for waveforms in Fig. 7(a) except for an increasing phase shift and the obvious difference in amplitude of high frequencies in the raw measurement. As visible on the spectra (figure 7(b)), the most basic simulation (F-P) presents a difference in inharmonicity and an important gap in amplitude of resonance peaks above 2 kHz. Another difference may be noticed about several resonance peaks visible in the measurement but absent of the simulation. For example, the amplitude of the second string partial which is well present in the measurement is approximately 16 dB lower in the modeled signal. This indicates the presence of phantom partials and clearly underlines the necessity for a nonlinear string model.

When the linear string model is replaced by the Kirchhoff-Carrier model, the inharmonicity of the simulation is fixed and subtle peaks appear in the vicinity of string modes, however the 16 dB difference around the second string mode is not rectified is visible in Fig. 7(c). To remedy this, the dynamic string tension presented in section II C is applied as an external force on the soundboard (after proper projection using $\theta_{b,8}$). This results
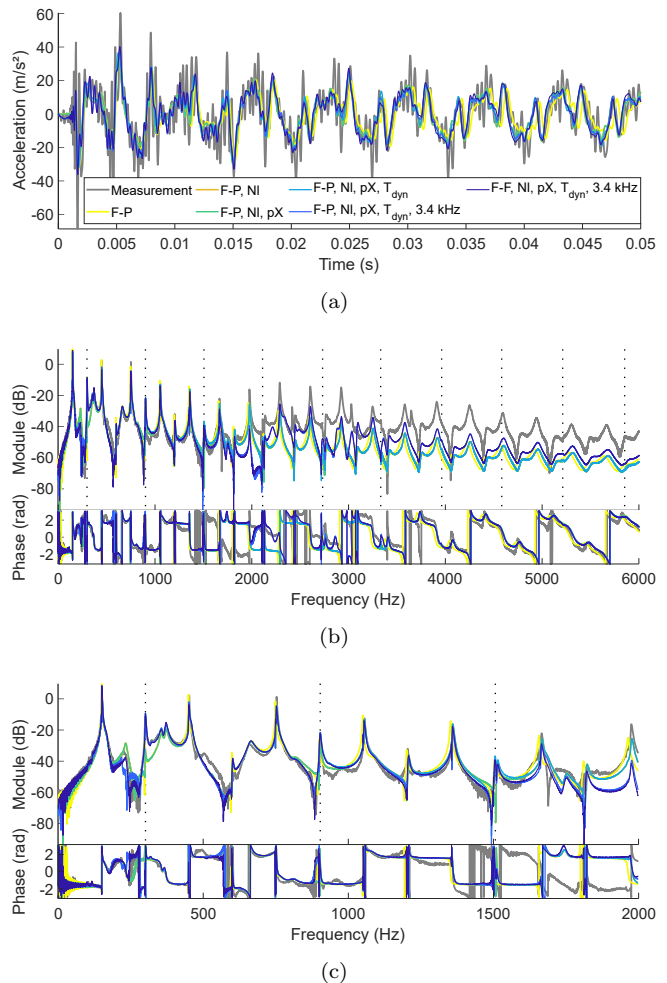

(a)

(b)

(c)

Figure 7. (Color online) Measurement/simulation comparison of soundboard acceleration at the attachment point of the 8th string plucked at the center in the direction Z with a breaking wire. (a) Waveforms; (b) Spectra; (c) Zoom of spectra between 0 and 1200 Hz. Vertical dashed lines indicate frequencies of even numbered phantom partials. F-P denotes a string/body coupling only at the soundboard; Nl denotes the inclusion of Kirchhoff-Carrier string model; pX denotes the presence of the transverse polarization X; T_{dyn} denotes the application of the dynamic string tension on the body; 3.4 kHz indicates the expansion of the modal basis of the body from a truncation at 1800 Hz to 3400 Hz; F-F denotes a string/body coupling at the soundboard (in the Z polarization) and the neck (in Z and X polarizations).

in the generation of some phantom partials which were missing up to now, indicated by vertical black dashed lines in Figs. 7(b) and 7(c), and the removal of the 16 dB gap previously mentioned. These observations highlight the validity of the approach presented in section II C 2.

In an attempt to correct the trend in the amplitude of string's resonances, the modal basis of the harp body

is expanded by including roughly identified modes in the frequency range [1.8, 3.4] kHz (no satisfying identification was achieved above 3.4 kHz). Indeed, the soundboard being driven by the force exerted by the string at the attachment point, an underestimation of the driving point accelerance will inevitably lead to an underestimation of its dynamic response. A study of the clavichord[19] based on the U-K formalism confirmed the strong influence of modal truncation on the high frequency content of physical simulations. As shown in Figs. 7(a) and 7(b), the same observation is made in the case of the Fang harp, it is clearly visible both in time and frequency domains despite the poor comparison between measured and reconstructed driving point accelerances (see Fig. 8). It should be noted that while the average spectral slope gets closer to the one of the measurement, the amplitude of some phantom partials is also substantially improved (for example at 2730 Hz, 3030 Hz) and at the same time undesired resonances appear in the frequency range of the added body modes.
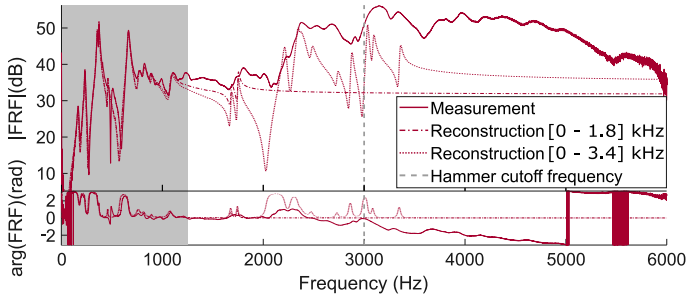

Figure 8. (Color online) Comparison between measured and reconstructed collocated accelerances on the soundboard at the attachment point of the 8th string.

Finally, the inclusion of string/neck coupling in the Z polarization only slightly improves the amplitude of string partials, at least for the configuration studied here as shown in Fig. 7(c). Indeed, as visible on mode shapes presented in Fig. 5, neck displacement is mainly small at the attachment point of the 8th string when soundboard shapes do not correspond to first rolling mode contributions. For the same reason, no improvement appears when a second transverse polarization is included especially since the plucking is contained in the string plane.

However, when considering case (ii) the influence of string/neck coupling is more pronounced. Figure 9 shows three simulations of the soundboard acceleration response at the 8th string attachment position against a measurement. When coupling only the X string polarization, body mode contributions at 218 Hz, 238 Hz, 356 Hz and 1210 Hz are improved but the amplitude of string partials seems rather unchanged. The coupling of the Z polarization appears to be the most influential given that in neatly corrects the 4th string partial amplitude whose modal frequency is in the vicinity of a strong resonance of the neck (795 Hz). Differences between simulation and measurement remain regarding the amplitude of string
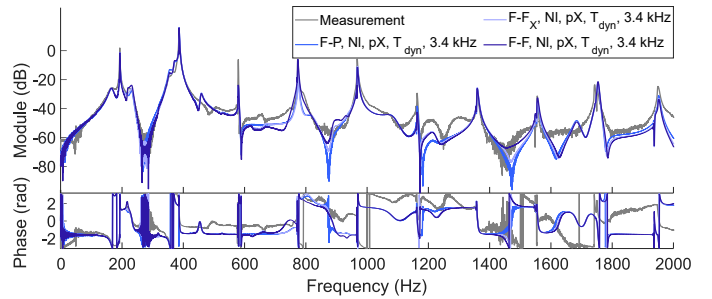

Figure 9. (Color online) Spectra of the soundboard acceleration at the attachment point of the 8th for a plucking applied on the 5th string at the third in the direction XZ with a breaking wire. F-F_X denotes a string/body coupling at the soundboard (in the Z polarization) and the neck (in the X polarization).

partials of order multiple of three which highlights the limits of the present implementation of string nonlinearities.

As a next step in assessing the model, case (iii) is investigated. Two model/measurement comparisons in the time-frequency domain are shown in Fig. 10 to study the relation between the plucking force and the generation of phantom partials. For all plucking forces, again a good agreement with the measurement is observed, however, differences in decay time are visible, especially in the vicinity of components where phantom partials are expected. Moreover, these differences in decay time go along with a beating in the measurement which is mostly well reproduced by the model for even numbered partials (indicated by white arrows) but absent for odd numbered partials (indicated by gray arrows) or masked by the linearly excited ones. The roughly identified body modes above 1800 Hz are probably part of the reason for this observation. Added to this is the efficient but simplistic string model proposed by Kirchhoff and Carrier that it would be interesting to compare to more elaborate models taking into account the spatial variation of the dynamic string tension. It is worth noting that, despite preceding observations, the harp model successfully represent the evolution of nonlinear phenomenon with the plucking force.

The final step deals with the assessment of pitch glide effects in the simulated response of the harp for case (iv). A comparison of spectrograms between modeled and measured acceleration signals is presented in Fig. 11(a). This representation clearly shows the presence of a dynamic string tension in the model which appears to be of the same order of magnitude as in the measurement. To give a better idea of the amount of pitch variation, a zoom on the 5th string partial is displayed in Fig. 11(b). It is noticeable that the model accurately represents the pitch variation induced by the increase in mean tension, at least for the range of excitation force investigated in this study which is up to 2 N. Important amplitude differences are visible for partials whose order is a multiple
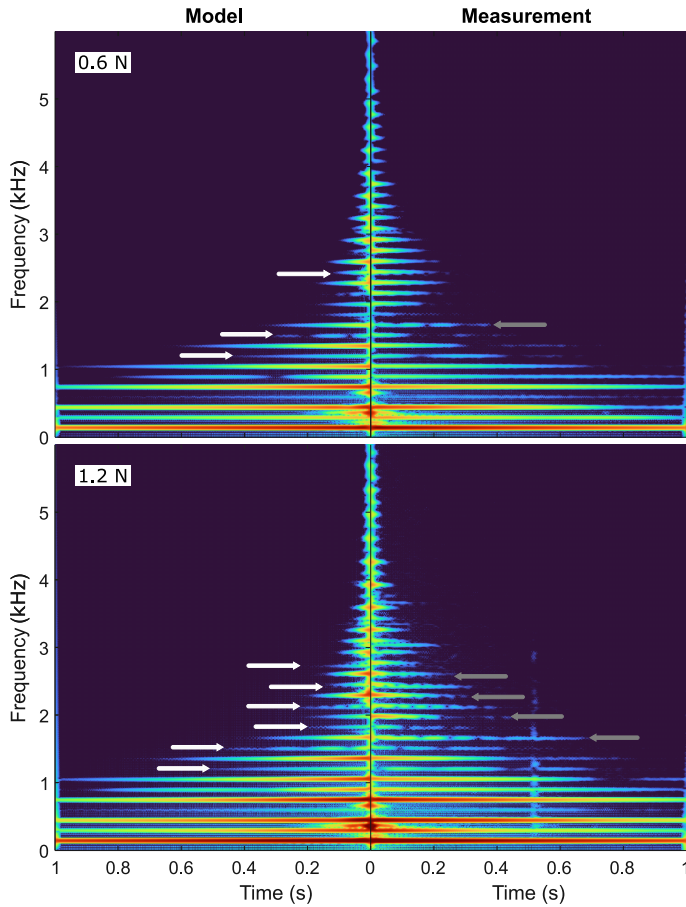
Figure 10. (Color online) Spectrograms of the soundboard acceleration at the attachment point of the 8th string plucked at the center with the finger in the direction Z for two plucking forces. White and gray arrows indicate, respectively, even numbered and odd numbered phantom partials. Each plot shows a range of 60 dB. The plucking force indicated in the top left corner of each comparison is estimated by adjusting the amplitude of the simulations to the measurement.

Figure 11. (Color online) Spectrograms of the soundboard acceleration at the attachment point of the 8th string plucked at the third with the finger in the direction XZ. (a) First 10 string partials; (b) Zoom on the 5th string partial. Each plot shows a range of 53 dB. The white dashed lines indicate the frequency of string partials just after the plucking to highlight the increasing shift with time.

of 3. Considering the plucking position, those components should not be present in the case of a linear string. This amplitude error thus probably indicates the limit of the Kirchhoff-Carrier approach.

V. CONCLUSION

This paper develops a physical model with a view to understanding the main features responsible for the sound signature of Central Africa harps. The instrument is treated as a multibody structure consisting in the strings and the body under point coupling using the modal U-K formalism. First, the mathematical framework of the model is presented, including the dynamics of the uncoupled subsystems as well as conditions of continuity at the soundboard and at the neck. A modal formulation of the Kirchhoff-Carrier string model allows to take into account string geometrical nonlinearities.
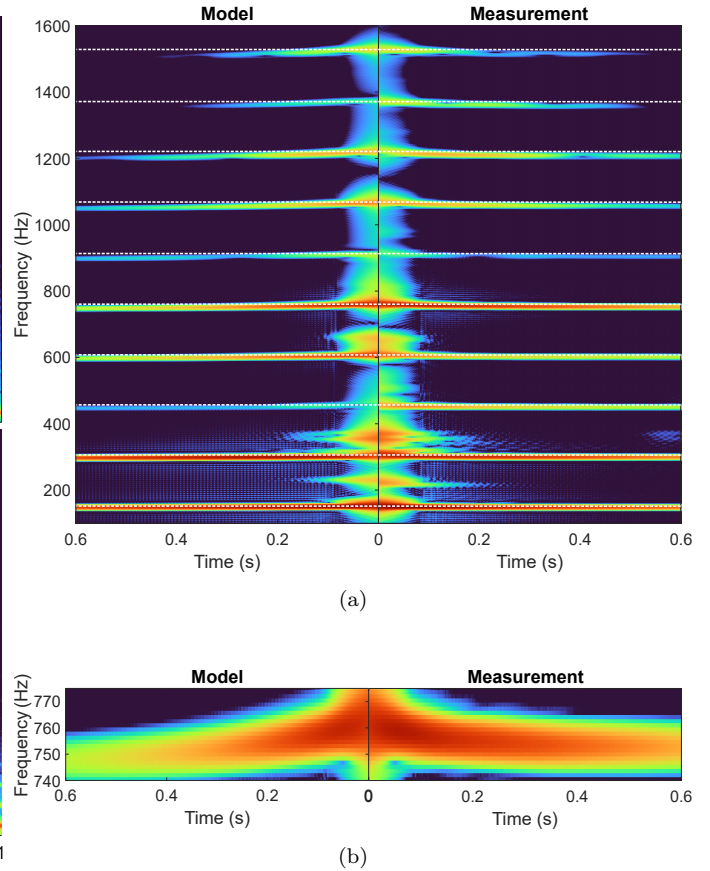
Details regarding strings and body modal parameters estimation procedure are then addressed with a special attention to the estimation of mode shapes and modal masses (as those details seem to be frequently missing in musical acoustic literature). Body modes experimentally identified, on a harp from the Fang ethnic group, reveal the presence of a well known vibroacoustic coupling between the soundboard and the air cavity. Moreover, the soundboard exhibits a membrane-like behavior while the neck is similar to a fixed-free beam.

Finally, numerical simulations are confronted with experimental data, for different levels of complexity, to assess the harp model. The inclusion of geometrical nonlinearities in the string behavior proves to be important on two aspects. First, it allows to accurately model the initial pitch glide in the string partials observed in the measurements. Secondly, it results in the generation of some phantom partials in the vicinity of linearly excited ones of odd number, as predicted by earlier studies of

piano strings. Most importantly, when the variation in mean string tension is applied on the body, a new set of phantom partials appears around even numbered string modes. This represents a first key point in this work and confirms published results regarding the influence of nonlinearly excited longitudinal string modes on the generation of phantom partials. Next, as already observed in a study of the clavichord, the truncation of the modal basis of the body highly affects the high frequency content of physical simulations. Lastly, the second key point of this paper lies in the technical achievement of including the string/neck coupling in two transverse polarizations using the modal U-K formalism. This coupling shows a strong influence when there is a coincidence between string and neck modal frequencies. Overall, the harp model is able to simulate waveforms in very good agreement with the measurement and already represents a useful tool to investigate characteristic features of Central Africa harps.

The present state of the model is promising and representative of several physical features of a harp from Central Africa. However, as reveled by the confrontation with the measurements, ways of improvements are still to be considered. The most obvious limitation comes from modal truncation, induced by difficulties during experimental modal analysis. There exists methods to correct effects introduced by modal truncation in other substructuring approaches and their adaptation to the U-K formalism would be definitively beneficial. It would also be interesting to implement other nonlinear string models in order to improve the amplitude of some phantom partials and compare their range of validity. Lastly, the current plucking model is very simple and a more realistic finger model should be implemented to accurately represent the interaction of the harpist with the instrument.

ACKNOWLEDGMENTS

REFERENCES

[1] S. Le Bomin, E. Lechaux, and M.-F. Mifune, "Ce que ≪ faire ensemble ≫ peut vouloir dire en musique" ("What ≪ doing together ≫ can mean in music"), Cahiers d'ethnomusicologie 21, 175–204 (2008).

[2] F. Borel, "Philippe Bruguière, Gaetano Speranza, ed. : La parole du fleuve. Harpes d'Afrique centrale" ("Philippe Bruguière, Gaetano Speranza, ed. : The word of the river. Harps from central Africa"), Cahiers d'ethnomusicologie 13, 229–231 (2001).

[3] J.-L. Le Carrou, D. Bedoya, M.-F. Mifune, and S. Le Bomin, "Acoustique des harpes d'Afrique centrale : Etude préliminaire" ("Acoustics of harps of central Africa: Preliminary study"), in 14ème Congrès Français d'Acoustique (CFA'18), Le Havre, France (April 23-27, 2018), pp. 249–254.

[4] C. Waltham, "Harp," in The science of string instruments, edited by T. D. Rossing (New York, Springer New York, 2010),

[5] C. Waltham, and A. Kotlicki, "Vibrational characteristics of harp soundboards," J. Acoust. Soc. Am. 124(3), 1774–1780 (2008).

[6] J.-L. Le Carrou, F. Gautier, N. Dauchez, and J. Gilbert, "Modelling of sympathetic string vibrations," Acta Acust. United Acust. 91(2), 277–288 (2005).

[7] J. Woodhouse, "The acoustics of a plucked harp string," J. Sound Vib. 523, 116669 (2022).

[8] X. Boutillon, J.-C. Radier, C. Valette, and M. Castellengo, "Etude expérimentale des cordes pourvues de raideur" ("Experimental study of stiff vibrating strings"), Comptes-rendus des séances de l'Académie des sciences. Série 2, Mécanique-physique, chimie, sciences de l'univers, sciences de la terre 298(19), 815–820 (1984).

[9] J.-L. Le Carrou, F. Gautier, and E. Foltête, "Experimental study of A0 and T1 modes of the concert harp," J. Acoust. Soc. Am. 121(1), 559–567 (2007).

[10] A. J. Bell, and I. M. Firth, "The directivity of the concert harp," Acta Acust. United Acust. 69(1), 26–30 (1989).

[11] J.-L. Le Carrou, Q. Leclere, and F. Gautier, "Some characteristics of the concert harp's acoustic radiation," J. Acoust. Soc. Am. 127(5), 3203–3211 (2010).

[12] N. Lynch-Aird, and J. Woodhouse, "Comparison of mechanical properties of natural gut and synthetic polymer harp strings," Materials 11(11), 2160 (2018).

[13] N. Lynch-Aird, and J. Woodhouse, "Mechanical Properties of Nylon Harp Strings," Materials 10(5), 497 (2017).

[14] J. Woodhouse, "On the synthesis of guitar plucks," Acta Acust. United Acust. 90(5), 928–944 (2004).

[15] F. E. Udwadia, and R. E. Kalaba, "A new perspective on constrained motion," Proc. R. Soc. Lond. A 439(1906), 407–410 (1992).

[16] F. E. Udwadia, "Equations of motion for mechanical systems: A unified approach," Int. J. Non-Linear Mech. 31(6), 951–958 (1996).

[17] J. Antunes, and V. Debut, "Dynamical computation of constrained flexible systems using a modal Udwadia-Kalaba formulation: Application to musical instruments," J. Acoust. Soc. Am. 141(2), 764–778 (2017).

[18] V. Debut, and J. Antunes, "Physical synthesis of six-string guitar plucks using the Udwadia-Kalaba modal formulation," J. Acoust. Soc. Am. 148(2), 575–587 (2020).

[19] J.-T. Jiolat, C. d'Alessandro, J.-L. Le Carrou, and J. Antunes, "Toward a physical model of the clavichord," J. Acoust. Soc. Am. 150(4), 2350–2363 (2021).

[20] J.-T. Jiolat, J.-L. Le Carrou, and C. d'Alessandro, "Whistling in the clavichord," J. Acoust. Soc. Am. 153, 338–347 (2023).

[21] J. Chabassier, "Modélisation et simulation numérique d'un piano par modèles physiques" ("Modeling and numerical simulation of a piano by physical models"), Ph.D. dissertation, Ecole Polytechnique X, Palaiseau, 2012.

[22] A. A. Shabana, "Forms of the dynamic equations," in Computational Dynamics (John Wiley & Sons, Ltd, 2010) pp. 177–210.

[23] G. Kirchhoff, Vorlesungen über Mechanik (Lectures on Mechanics), (BG Teubner, Liepzig, 1883).

[24] G. F. Carrier, "On the non-linear vibration problem of the elastic string," Q. Appl. Math. 3(2), 157–165 (1945).

[25] B. Bank, and L. Sujbert, "Generation of longitudinal vibrations in piano strings: From physics to sound synthesis," J. Acoust. Soc. Am. 117(4), 2268–2278 (2005).

[26] M. Karjalainen, J. Backman, and J. Polkki, "Analysis, modeling, and real-time sound synthesis of the kantele, a traditional Finnish string instrument," in 1993 IEEE International Conference on Acoustics, Speech, and Signal Processing, Minneapolis, MN, USA (1993), Vol 1, pp. 229–232.

[27] P. Guillaume, P. Verboven, S. Vanlanduit, H. Van Der Auweraer, and B. Peeters, "A poly-reference implementation of the least-squares complex frequency-domain estimator," in Proceed-

ings of IMAC, Kissimmee, FL, USA (February, 2003), Vol. 21, pp. 183–192.

[28] J. Piranda, "Analyse modale expérimentale" ("Experimental modal analysis"), Techniques de l'ingénieur **RD2**(R6) 1-29 (2001).

[29] C. Valette, and C. Cuesta, *Mécanique de la corde vibrante* (*Mechanics of vibrating string*), Traité des nouvelles technologies, série Mécanique (Hermes, Paris, 1993).

[30] J. Woodhouse, "Influence of damping and nonlinearity in plucked strings: why do light-gauge strings sound brighter?," Acta Acust.

United Acust. **103**(6), 1064–1079 (2017).

[31] J.-L. Le Carrou, D. Chadefaux, L. Seydoux, and B. Fabre, "A low-cost high-precision measurement method of string motion," J. Sound Vib. **333**(17), 3881–3888 (2014).

[32] R. Roy, and T. Kailath, "ESPRIT-estimation of signal parameters via rotational invariance techniques," IEEE Trans. Acoust. Speech Signal Process **37**(7), 984–995 (1989).

[33] A. Paté, J.-L. Le Carrou, and B. Fabre, "Predicting the decay time of solid body electric guitar tones," J. Acoust. Soc. Am. **135**(5), 3045–3055 (2014).